Efficient molecule discrimination in electron microscopy through an optimized orbital angular momentum sorter

F. Troiani,[1] E. Rotunno,[1,*] S. Frabboni,[1,2] R. B. G. Ravelli,[3] P. J. Peters,[3] E. Karimi,[4] and V. Grillo[1]

[1]*Centro S3, CNR-Istituto di Nanoscienze, via Giuseppe Campi 213/A, I-41125 Modena, Italy*

[2]*Dipartimento di Scienze Fisiche, Informatiche e Matematiche, Università di Modena e Reggio Emilia, via Giuseppe Campi 213/A, I-41125 Modena, Italy*

[3]*The Institute of Nanoscopy, Maastricht University, 6211 LK Maastricht, Netherlands*

[4]*Department of Physics, University of Ottawa, Ottawa, Ontario, Canada K1N 6N5*

(Received 10 February 2020; revised 29 July 2020; accepted 9 September 2020; published 12 October 2020)

We reformulate the single-molecule analysis in an electron microscope in terms of a quantum-state discrimination problem, and discuss its implementation through electron-beam shaping. Our approach relies on the use of new electron-optical elements to efficiently extract the "which-molecule" information from the state of each electron. The optimal observables are formally derived, and subsequently implemented by suitably designed phase elements in a generalized orbital angular momentum sorter. As a representative example, we simulate the discrimination between model proteins and benchmark the performance of the sorter against that of the best known real-space approach.

DOI: 10.1103/PhysRevA.102.043510

I. INTRODUCTION

The quest for extreme sensitivities in the investigation of atomic and molecular systems naturally leads to the use of single particles as quantum probes. The state of such probes supposedly displays a strong dependence on the system under investigation, and can thus lead to an efficient inference on the system of interest. However, the use of single-particle probes also implies inherent limitations, resulting from fundamental quantum features, such as decoherence and the measurement postulate [1]. Decoherence tends to smear out the information encoded in the particle state, while the measurement postulate implies the impossibility of discriminating two nonorthogonal states [2]. A full account of these quantum aspects is thus required in order to identify the optimal measurement strategy.

In electron microscopy the quantum probe is represented by the electron [3]. The measurement process implies the "collapse" of its wave function, which reduces to a pixel on a detector. A full image of the sample is obtained by using a large number of electrons, whose distribution on the detector represents the measurement statistics [4,5]. However, in order to limit the damage induced in the investigated system, the number of electrons used in the imaging process should be minimized [6], especially in beam-sensitive objects such as proteins. This has fueled the development of novel techniques such as cryomicroscopy and single-particle analysis [3]. However, these techniques require the imaging of many supposedly identical proteins, while the accurate imaging of a single protein remains largely prohibitive. The recent introduction of beam shaping techniques [7,8] has allowed the application to electron microscopy of concepts originally developed in quantum optics. In particular, through the use of appropriate electrostatic elements [9–11] or holograms [12], one can implement the measurement of different observables. The most considerable case is the recently demonstrated orbital angular momentum (OAM) sorter [13,14], which permits a direct measurement of the orbital angular momentum. The large flexibility that this approach allows in the choice of the measured observable represents a key resource for maximizing, in a system-specific fashion, the amount of information that can be extracted from the electron wave function, thus reducing the number of probes that are required to achieve a given degree of confidence in the final inference.

In the present article, we consider the problem of discriminating between two molecules by means of an OAM sorter. We formalize the problem within the general framework of quantum-state discrimination [15,16]. This enables the derivation of the optimal measurement strategy, both in the ideal case of a full knowledge of the alternative molecule states and of a coherent electron dynamics, and in the more general case where the state of the molecule is partially unknown and/or the electron dynamics is affected by decoherence [17]. We identify the optimal strategy with a correlated measurement of the radial and angular degrees of freedom of the electron wave function, which maximizes the "which-molecule" information extracted from the electron. In particular, we show that the OAM sorter implements the optimal measurement strategy in the representative cases of decoherence in the angular degrees of freedom or of a complete lack of knowledge of the protein in-plane orientation. The lack of knowledge concerning the in-plane orientation of the molecule is common in experiments, and its effect can be accounted for by the use of mixed electron states. Decoherence in these experiments can typically result from the presence of specific inelastic channels, such as those represented by "azimuthal" plasmon modes [18]. Here we

*enzo.rotunno@nano.cnr.it

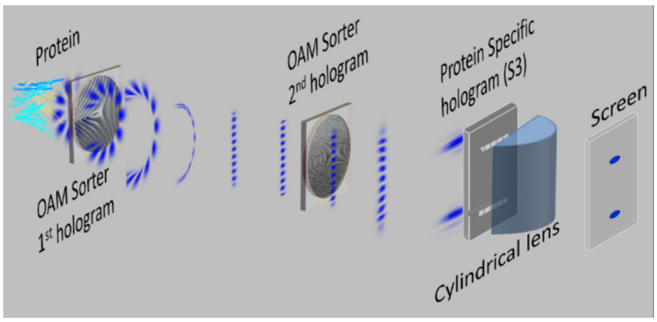

FIG. 1. Schematic view of the generalized OAM sorter. A transmission electron microscope (TEM) projection system is modified as for an OAM sorter; in addition, a third phase element is included to produce a generalized OAM sorter. The structure of such third element is adapted to the radial structure of the eigenstates $\chi_{0,m}$ and $\chi_{1,m}$ corresponding to the angular momentum component m.

show that, also in these cases, the optimal measurement can be implemented by including in the OAM sorter additional electron-optical elements, which lead to the measurement of the radial degree of freedom. We refer to such device as the *generalized OAM sorter* (Fig. 1).

The paper is organized as follows. In Sec. II we introduce the general formalism and main figure of merit, derive its expression in the cases of complete and incomplete knowledge of the state of the molecules to be discriminated, and then focus on the discrimination by means of an OAM sorter, by means of one or more electrons. In Sec. III we simulate the discrimination between protein models, which we consider as representative examples. Finally, in Sec. IV we draw the conclusions.

II. DISCRIMINATION BETWEEN TWO MOLECULES

In this section, we first formalize the process by which the information on the molecule identity and state is encoded in the state of each individual electron. We then introduce the figure of merit that is used to rate the measurement strategy, namely, the discrimination probability, and recall (derive) its expression in the case of a pure (mixed) electron state.

A. Encoding the information on the molecule state on the electron state

The prototypical problem of discriminating between two molecules can be formalized as follows [16,19]. One considers two hypotheses $I_k (k = 0, 1)$; each one specifies the molecule identity (X_k) and orientation, and is assigned an *a priori* probability p_k. After the interaction with the molecule, the electron that is used as a probe is left either in the state $|\psi_0\rangle$ or in $|\psi_1\rangle$, depending on which of the two hypotheses applies. A measurement is eventually performed in order to identify the electron state and thus to infer the correct I_k.

For the sake of the following discussion, it is convenient to expand the two alternative electron states in terms of the normalized projections $|m, \chi_{k,m}\rangle$ on the eigenspaces of the OAM, namely, $L_z = -i\hbar\frac{\partial}{\partial\varphi}$ (here z is the electron-propagation direction, φ is the azimuthal angle in the plane orthogonal to z, $\hbar$ is the reduced Planck constant, and m is the integer OAM quantum number):

$$|\psi_k\rangle = \sum_m \sqrt{q_{k,m}}|m, \chi_{k,m}\rangle, \tag{1}$$

where q_m ($\sum q_m = 1$) is the probability associated with each value m of L_z. The symbols $\chi_{k,m}$ denote the radial wave functions associated with a certain molecule (specified by k) and with a given value of m (in general these functions do not form a complete basis and do not need to be mutually orthogonal).

The association of a pure electron state with each of the two hypotheses is based on the assumption that the electron dynamics is not affected by decoherence and that the molecule state is perfectly defined within each I_k. If the molecule state is partially unknown and/or the electron is affected by decoherence, the state vectors $|\psi_k\rangle$ are replaced by density operators ρ_k. In particular, if the molecule is centered at the optical axis and its orientation around the z axis is undefined, the density operators are obtained by an incoherent averaging of the pure-state density matrix over the different orientations:

$$\rho_k = \sum_m q_{k,m}|m, \chi_{k,m}\rangle\langle m, \chi_{k,m}|, \tag{2}$$

where all the information that was contained in the relative phases between $|m, \chi_{k,m}\rangle$ components has been erased (the methods and limitations in experimentally centering the molecule at the optical axis are described in Sec. III). We note in passing that the same effect can be produced by the electron decoherence, if this affects the phase coherence between different eigenstates of L_z.

In the following, we simulate the electron dynamics within the microscope in order to derive the expressions of the pure (mixed) states $|\psi_k\rangle$ (ρ_k) that correspond to a few representative protein models.

B. Expression of the discrimination probability

The discrimination between the two electron states is performed on the basis of the measurement outcome. In particular, one identifies two outcomes whose occurrence makes more likely either one hypothesis or the other. Formally, each outcome is associated with a probability operator Π_k, whose expectation value gives the probability that the kth outcome occurs. The probability of identifying the correct hypothesis on the basis of a single-electron measurement is thus given by [14,15]

$$p = p_0 \mathrm{tr}(\rho_0\Pi_0) + p_1 \mathrm{tr}(\rho_1\Pi_1), \tag{3}$$

where the first (second) term represents the probability that the first (second) hypothesis is true and that the measurement provides the corresponding outcome $k = 0$ ($k = 1$). The probability p is the figure of merit we use in the following to rate the measurement strategy, and can be maximized by a suitable choice of the observables. The optimal observables are the ones that, for a given pair of molecules and (thus) of states of the electron, maximize p.

There is, however, a fundamental limitation related to the quantum nature of the probe: If the two electron states are not orthogonal, there is no quantum measurement that can perfectly discriminate them [2]. In fact, in the case of two pure states, the probability p cannot exceed the Helstrom bound

[15],

$$p^{\psi}_{\max} = \tfrac{1}{2} + \tfrac{1}{2}[1 - 4p_0 p_1 |\langle\psi_0|\psi_1\rangle|^2]^{\frac{1}{2}}, \tag{4}$$

which ranges from $\frac{1}{2}$ to 1 as the overlap between the two states varies from 1 to 0. The value of $\frac{1}{2}$ corresponds to the blind guess case, where there is no *a priori* information on the molecule identity ($p_0 = p_1 = \frac{1}{2}$) and the electron state carries no which-molecule information (the states $|\psi_0\rangle$ and $|\psi_1\rangle$ coincide). In general, the lower the which-molecule information encoded in the molecule state, the larger the overlap between the two electron states, and the smaller the upper bound $p^{\psi}_{\max}$ of the discrimination probability. For a given pair of electron states, the optimal measurement strategy is the one that leads to a discrimination probability $p = p^{\psi}_{\max}$.

In passing from pure ($|\psi_k\rangle$) to mixed (ρ_k), the electron states tend to become less distinguishable and the probability of discriminating between the two hypotheses thus tends to decrease. The upper bound is thus given by [16]

$$p^{\rho}_{\max} = \frac{1}{2} + \frac{1}{2}\sum_m [(p_0 q_{0,m} + p_1 q_{1,m})^2 - 4p_0 p_1 q_{0,m} q_{1,m} |\langle\chi_{0,m}|\chi_{1,m}\rangle|^2]^{\frac{1}{2}} \leqslant p^{\psi}_{\max}. \tag{5}$$

The above limits can be achieved by identifying and implementing the quantum measurement that is optimal, given the electron states ρ_k and the *a priori* probabilities p_k. Therefore, the value of the upper bound quantifies the amount of which-molecule information encoded in the electron states, while the ratio between the discrimination probability p and the upper bound quantifies the capability of a particular measurement to extract such information from the electron state.

C. Discrimination probability with the generalized OAM

For a given measurement, the discrimination probability p can be maximized by assigning each outcome to one of the two hypotheses, according to a maximum likelihood criterion [15]. Within our approach, the electron is sorted on the basis of the OAM value m; a measurement of the radial degrees of freedom is then performed, on a basis that can in general be different for each m. This corresponds to a correlated measurement of the radial and angular degrees of freedom, which can be formalized through the probability operators $\pi_{k,m} (k = 0, 1)$, each corresponding to a specific outcome. The resulting expression of the discrimination probability reads

$$p^{\rho}_{\mathrm{OAM}} = p^{\psi}_{\mathrm{OAM}} = \sum_m \max\{p_0 q_{0,m} \langle\chi_{0,m}|\pi_{0,m}|\chi_{0,m}\rangle, p_1 q_{1,m} \langle\chi_{1,m}|\pi_{1,m}|\chi_{1,m}\rangle\} \equiv p_{\mathrm{OAM}}. \tag{6}$$

As pointed out in the first equality, the discrimination probability is unaffected by the loss of phase coherence between the different angular momentum components. This reflects the fact that, within this approach, the which-molecule information is encoded in degrees of freedom that are unaffected by the considered dephasing process. This measurement strategy can always be made optimal by identifying the proper electrostatic elements in our generalization of the OAM sorter (see the detailed description below and in the Appendix). For a given pair of molecules, the optimal elements can be deduced from the calculated expression of the optimal observables $\pi_{0,m}$ and $\pi_{1,m}$, which correspond to the projectors on eigenstates $\lambda_{1,2}$ of $\sigma_m \equiv \sum_{j=0,1} (-1)^j p_j q_{j,m} |\chi_{j,m}\rangle\langle\chi_{j,m}|$ with positive and negative eigenvalues, respectively. (Counterintuitively, the optimal discrimination between two states with a large overlap is achieved by projectors on states that do not coincide with $\chi_{0,m}$ and $\chi_{1,m}$, but on highly mixed combinations of these two states.) The optimal observables are implemented by suitable combinations of phase elements, which we derive in our simulations.

D. Discrimination based on multiple electron measurements

So far we have considered the limiting case where the discrimination between the hypotheses I_0 and I_1 is performed on the basis of a single-electron measurement. The probability p of identifying the correct hypothesis can be increased by repeating such measurement N times, one on each of the electrons that has interacted with the molecule.

If a two-outcome measurement is repeated N times, the overall measurement presents 2^N possible outcomes. We consider as equivalent sequences that correspond to the same numbers, n_0 and n_1 (where $n_0 + n_1 = N$), of outcomes 0 and 1, independently of the order in which these have occurred. Therefore, the probability that the outcome 0 occurs n_0 times, if the hypothesis I_k applies, is given by the binomial distribution

$$S_k(n_0, n_1) \stackrel{\mathrm{def}}{=} \binom{N}{n_0} [\mathrm{tr}(\rho_k \Pi_0)]^{n_0} [\mathrm{tr}(\rho_k \Pi_1)]^{N-n_0}. \tag{7}$$

According to a maximum likelihood criterion and along the lines of what has been done above for the single-electron case, the occurrence of n_0 outcomes 0 is related to either I_0 or I_1, depending on whether $S_0(n_0, n_1)$ is larger or smaller than $S_1(n_0, n_1)$. After summing over all the possible values of n_0, from 0 to N, one obtains the expression of the discrimination probability for the N-electron case, which is given by

$$P(N) = \sum_{n_0=0}^{N} \binom{N}{n_0} \max\left\{p_0 s_0^{n_0} (1 - s_0)^{N-n_0}, p_1 s_1^{n_1} (1 - s_1)^{N-n_1}\right\}. \tag{8}$$

Here, the success probabilities are s_0 or s_1, depending on whether I_0 and I_1 apply, with $s_k \equiv \mathrm{tr}(\rho_k \Pi_k)$. From this expression of $p(N)$ one can derive the minimum number of electrons that are required in order to exceed a given threshold $x : p(N) > x$ for $N \geqslant N_{\min}(x)$.

III. TEST CASE: DISCRIMINATION BETWEEN TWO PROTEINS

Hereafter, we apply the above approach to the discrimination of two proteins. In particular, we simulate the electron states ($|\psi_k\rangle$ or ρ_k) in the presence of each protein, derive the optimal phase plate elements, and compute the corresponding discrimination probability. The measurement performed by means of the generalized OAM sorter is schematically represented in Fig. 1. The electron is prepared in a plane-wave state (that propagates along the z direction), before interacting with the protein. An appropriate cutoff (a circular aperture

25–50 nm in diameter) is added to the plane wave in order to illuminate only the specific protein but large enough so as to not interfere with the recognition process. Typically we can use the condenser system to concentrate the beam down to a few tens of nanometers with negligible convergence. Such interaction perturbs the electron state in a way that depends on the protein identity and state. Suitably engineered phase elements then direct state components corresponding to different values of L_z to different regions of the detector, thus implementing a measurement of the orbital angular momentum. The phase elements induce a conformal transformation from Cartesian to log-polar coordinates; a further diffraction permits one to measure the conjugated quantities OAM and logarithmic radial momentum. The OAM and radial momenta are always defined with respect to a center (i.e., the optical axis of the microscope) and it is therefore necessary to make sure that the molecule is correctly positioned. This can be done with low magnification imaging that requires a very limited dose or with the correlative use of techniques as with correlative light electron microscopy (CLEM [20,21]).

Here, additional phase elements beyond the standard OAM sorter are introduced, which further sort each angular momentum component on the basis of its radial state through a *phase-flattening* technique. The phase elements are adapted in order to match and conjugate the phase along the radial degree of freedom. A cylindrical lens (produced in electron microscopy by the combination of stigmators and round lenses) can then be used to obtain a further diffraction of the sole radial degree of freedom, while the OAM channels are unaffected and remain well separated. A similar configuration (without the third phase element) is used to sort on an OAM Bessel representation of the wave function [22]. After phase flattening, the radial wave function for each OAM channel has a constant (flattened) phase, which diffracts a specific OAM channel state to a relatively narrow spot [23]. If the matching is not perfect, the resulting phase of the wave function oscillates and the diffraction is much more diffuse. The procedure could in principle be further improved by manipulating and flattening the amplitude of the wave function, but this is experimentally much more challenging.

In the standard OAM sorter, the radial diffraction produces a very sparse representation of the electron wave function for a given target molecule. These additional phase elements are therefore specific to each discrimination problem and implement the optimal projectors [see Eq. (6) and related discussion]. As discussed above, such optimization is specific to the pair of molecules, rather than to an individual molecule. Therefore, the "phase-flattening" process is not tuned on one of the two proteins to be discriminated, but on a specific combination λ_1 (or λ_2) [obtained in Eq. (6)] that maximizes the discrimination probability.

In an alternative strategy, both the matching of the phase on λ_1 or on λ_2 can be chosen. As a result the diffraction will be peaked for one protein and diffuse for the other or vice versa.

It is worth mentioning that the role of the additional third element is to make the representation of the protein sparse, ideally to a single point. This is of practical use to overcome camera shot noise and simplify the overall experiment.

The electron wave function, and in particular its transverse (x, y) component ψ_k, is affected by the interaction with the protein X_k, and becomes [3,24]: $\psi_k(x, y) = A_k(x, y)\exp[iCV_k(x, y)]$. Here, V_k is the atomic electrostatic potential induced by the protein, which modulates the phase and, to a minor extent, the amplitude of the electron wave function, and $C = 2\pi m_0 \gamma \lambda/\hbar^2$ (where m_0 is the electron rest mass, γ the relativistic factor, λ the wavelength, and $\hbar$ the Planck constant). Since the proteins consist of light elements, the phase modulation is typically small ($CV \ll \pi$). We compute the protein-specific potentials V_k, the corresponding electron states (ψ_k or ρ_k), and, from these, all the relevant quantities that appear in the above equations (1)–(6).

As a representative example, we consider the two-by-two discrimination between three model proteins, all referring to the EspB protein of *Mycobacterium tuberculosis*. The first two models, hereafter labeled P_a and P_b, are characterized by the same (sevenfold) rotational symmetry [25,26], which differs from that (sixfold) of the third model (P_c). These examples are significant because these models are hardly distinguishable from one another experimentally. Besides, the discrimination between P_c and the other two models is qualitatively different from that between P_a and P_b, since it relies also on the azimuthal—rather than on the radial—degree of freedom.

The simulation of the spectra that are relevant for the protein discrimination, based on the use of the optimal observables, is reported in Fig. 2 for the case of P_a and P_b. The simulations refer to the case of limited doses (2 and $0.2\,e/\text{Å}^2$) and low acceleration voltages (60 kV), and are performed by double-extraction Monte Carlo methods. As expected for the case of strongly overlapping (electron) states ρ_0 and ρ_1, the optimal radial observables give rise to overlapping outcome probability distributions [19]. This is particularly clear for the $m = 0$ subspace [panels (c) and (f)], where the largest component of the electron wave functions is concentrated. Here, following a maximum likelihood criterion, each measurement outcome is assigned to the hypothesis I_0 (protein P_a) if the outcome probability in the presence of P_a (green curve) is larger than that in the presence of P_b (red curve), and to the hypothesis I_1 (protein P_b) otherwise. (We have highlighted in a binary histogram which region should be assigned to the first or second hypothesis.) If the discrimination is based on more than one electron detection, the decision is based on the approach outlined in Sec. II D. We note that, unlike what happens in a real-space case, the spectra obtained by means of the OAM sorter coincide for the pure and mixed electron states, and are thus unaffected by undefined protein orientation or decoherence [17].

The effect of the observable optimization is not immediately evident by looking at the spectra, but can be quantitatively appreciated by deriving the discrimination probability from the simulated measurement outcomes (Table I). We start by quantifying the which-protein information encoded in the electron state. This is quantified by the overlap $|\langle\psi_0|\psi_1\rangle|$ between the electron wave functions corresponding to the two hypotheses, which is close to 1 for all pairs of proteins (columns 2–4). A single-electron probe thus carries a very limited amount of which-protein information, which leads to a maximal discrimination probability ($p^{\psi}_{\max}$) that is a few cents above the "blind-guess" value of $\frac{1}{2}$, and is further reduced ($p^{\rho}_{\max}$) by decoherence.

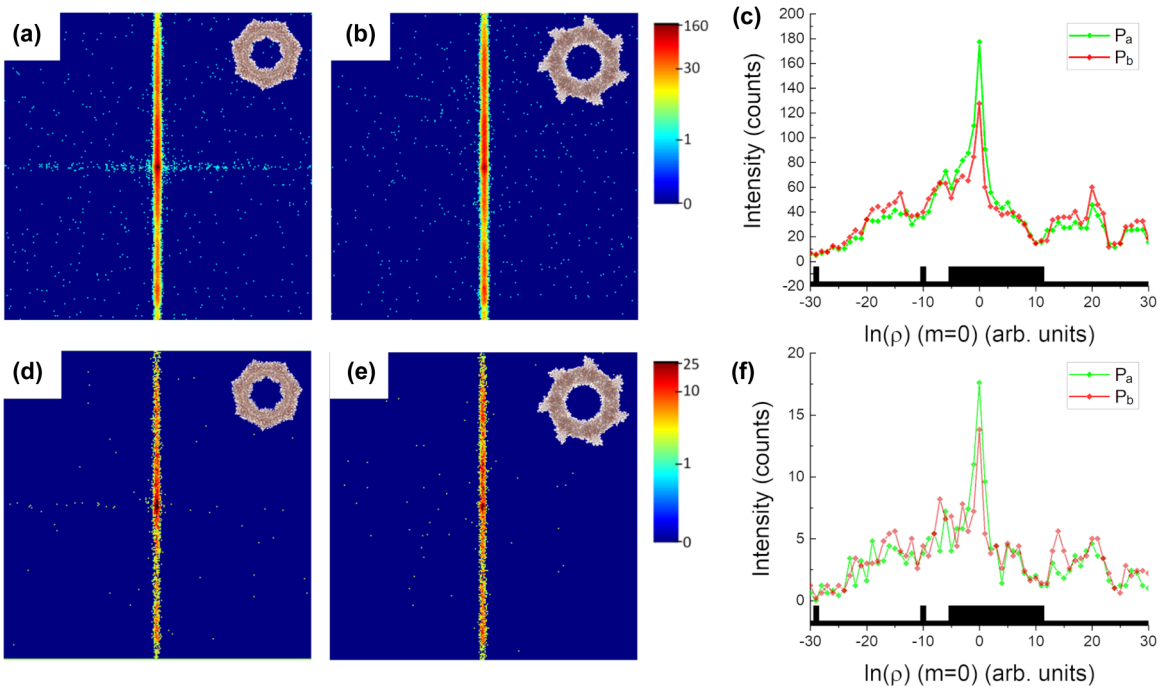

FIG. 2. Simulated spectra with phase elements optimized for discriminating between the proteins P_a and P_b. The upper and the lower panels correspond, respectively, to doses of 2 and 0.2 $e^-/\text{Å}^2$. The proteins P_a (a), (d) and P_b (b), (e) give rise to different distributions of the electrons in the angular momentum (horizontal axis) and radial (vertical axis) bases. (c), (f) Detail corresponding to the radial observable for the $m = 0$ subspace, where the electron states are mainly concentrated. The black histogram below the plots specifies the outcomes for which the presence of the protein P_a is more likely than that of P_b.

We then quantify the suitability of the different measurements to access such which-protein information, by means of the corresponding probabilities p (columns 5 and 6). For the imaging in real-space (RS), we considered an ideal Zernike phase plate [27,28].

An ideal Zernike phase plate introduces a $\pi/2$ phase shift at the center of the diffracted image, thus generating constructive interference between scattered and background electrons and enhancing the image contrast. Its effect can be simulated by shifting by $\pi/2$ the central pixel of the Fourier transform of the wave function and then transforming back to real-space. We note that such phase shift has never been exactly realized in practice [29], so that the reported values should be regarded as upper bounds for this approach. Even in such ideal case, the values of the discrimination probabilities for the mixed states (p^{ρ}_{RS}) fall below the corresponding theoretical maxima. The optimal observables implemented through the OAM sorter lead to values of the discrimination probabilities (p_{OAM}, calculated using the maximum likelihood criterion described above) that are comparable and in most cases significantly larger than those achieved with the ideal Zernike phase plate. The small difference between p_{OAM} and the theoretical maximum p^{ρ}_{max} is possibly due to imperfections in the phase-flattening-based implementation of the optimal projectors $\pi_{k,m}$.

The maximal suitability of the implemented values of $N(x)$, all of the order of 10^2, correspond to doses of much less than 0.1 $e/\text{Å}^2$ (columns 7–9). This number is quite small and typically at least 50% better than in the case of the ideal Zernike phase plate. A limited amplification of the phase modulation (obtained, e.g., by using thicker proteins or multipass approaches [30]) would further highlight the advantage resulting from the use of optimal observables. Moreover, with a typical affordable dose of a few $e/\text{Å}^2$, something like 100 tests between different pairs of model proteins could be carried out simply by changing the phase of the final sorting element

TABLE I. Discrimination probabilities based on the use of a single-electron probe and corresponding to different pairs of proteins (X_0, X_1). The probabilities with superscript ψ and ρ correspond to the case of pure and mixed electron states, respectively; the subscripts max, RS, and OAM identify the theoretical maxima, measurements performed in real-space (with an ideal Zernike phase plate), and with the optimized OAM approach. In all the considered cases, the *a priori* probabilities are assumed equal ($p_0 = p_1 = \frac{1}{2}$). The values of N_{RS} and N_{OAM} are the number of electrons that are necessary to achieve a discrimination probability p higher than $x = 0.9$ with the two approaches. The last column indicated the corresponding dose for the OAM.

X_0, X_1	$\lvert\langle\psi_0\rvert\psi_1\rangle\rvert$	p^{ψ}_{max}	p^{ρ}_{max}	p^{ρ}_{RS}	p_{OAM}	$N_{\text{RS}}(x)$	$N_{\text{OAM}}(x)$	Dose ($1/\text{Å}^2$)
P_a, P_b	0.987	0.582	0.580	0.531	0.541	346	224	0.007
P_a, P_c	0.981	0.598	0.596	0.540	0.564	257	98	0.003
P_b, P_c	0.975	0.612	0.610	0.552	0.559	143	108	0.003

in a programmable way [31]. This implies a high degree of flexibility in the implementation of the OAM-based approach, and suggests the possibility to use adaptive learning in cases where the possible identities of the protein (molecules) are not limited to two options.

IV. CONCLUSIONS

In conclusion, we have investigated the problem of optimizing the discrimination between two molecules by means of electron microscopy. The discrimination procedure has been investigated within the framework of quantum-state discrimination, which allows one to fully account for the quantum nature of the electron. The discrimination process based on the use of the angular momentum sorter is robust with respect to decoherence affecting the electron and to the uncertainty on the protein orientation. We have shown that the generalized OAM sorter, which implements a correlated measurement of the radial and angular degrees of freedom, can in principle realize an optimal discrimination strategy, and have discussed, as a representative example, the case of the discrimination between model proteins. The observable optimization represents a fundamental means for minimizing the number of electrons that are required for the discrimination, and thus for limiting the induced damage.

The implementation of the protein recognition strategy will potentially bring advantage to cryomicroscopy, as an alternative or complementary method. We also suggest it could work in synergy with CLEM, where light and electron microscopies are used, respectively, to localize specific proteins of interest and to visualize all kinds of proteins with high resolution, in isolation or in their cellular context.

ACKNOWLEDGMENTS

This work is supported by Q-SORT, a project funded by the European Union's Horizon 2020 Research and Innovation Program under Grant Agreement No. 766970- Q-SORT (H2020-FETOPEN-1-2016-2017). We acknowledge Abril Gijsbers, Ye Gao, and Axel Siroy (UM) for having provided the EspB model. E.K. acknowledges the support of a Canada Research Chair and Ontario's Early Researcher Award.

APPENDIX A: EFFECT OF DECOHERENCE AND/OR OF THE UNDEFINED PROTEIN ORIENTATION

The state of the electron, in the case where the hypothesis I_k applies, is $|\psi_k\rangle$. We expand it in terms of the normalized projections $|m, \chi_{k,m}\rangle$ on the eigenspaces of the angular momentum L_z:

$$|\psi_k\rangle = \sum_m \sqrt{q_{k,m}}|m, \chi_{k,m}\rangle,$$

where $0 \leqslant q_m \leqslant 1$ is the probability associated with each value m of the angular momentum and $\chi_{k,m}$ accounts for the radial degree of freedom. The above state can be expanded on a complete and orthonormal basis $|m, p\rangle$ as follows,

$$|\psi_k\rangle = \sum_{m,p} c_{m,p}|m, p\rangle,$$

where $c_{m,p}$ are complex coefficients. The correspondence between the two representations is given by the equation

$$|\chi_{k,m}\rangle = \frac{1}{\sqrt{\sum_p |c_{m,p}|^2}} \sum_p c_{m,p}|p\rangle.$$

The initial electron state $|\psi_{\text{probe}}\rangle$ corresponds to a plane wave, traveling along the z axis. The anisotropic dependence of the states $|\psi_k\rangle$ on the azimuthal angle φ thus results from the interaction with the protein. A rotation of the protein with respect to a reference orientation by an angle δ induces a change $m\delta$ in the phase of $|m, \chi_{k,m}\rangle$. If the orientation of the protein around the z axis is completely undefined (i.e., any value of the angle δ in the range $[0,2\pi]$ is equally probable), the state of the electron is given by the statistical mixture

$$\begin{aligned}\rho_k &= \sum_{m,m'} \sqrt{q_{k,m}q_{k,m'}}|m, \chi_{k,m}\rangle\langle m, \chi_{k,m}|\frac{1}{2\pi}\int d\delta e^{i(m-m')\delta} \\ &= \sum_m q_{k,m}|m, \chi_{k,m}\rangle\langle m, \chi_{k,m}|.\end{aligned}$$

The loss of the information encoded in the phases tends to make the two alternative electron states less distinguishable. This can be verified by comparing the fidelities of the two pure states with that of the mixed ones:

$$\begin{aligned}\mathrm{F}(|\psi_0\rangle, |\psi_1\rangle) &= \left|\sum_m \sqrt{q_{1,m}q_{0,m}}\langle\chi_{1,m}|\chi_{0,m}\rangle\right| \\ &\leqslant \sum_m \sqrt{q_{1,m}q_{0,m}}|\langle\chi_{1,m}|\chi_{0,m}\rangle| = F(\rho_0, \rho_1),\end{aligned}$$

the fidelity by definition, being $F(\rho, \sigma) = \mathrm{tr}\sqrt{\rho^{1/2}\sigma\rho^{1/2}}$.

APPENDIX B: THEORETICAL MAXIMUM OF THE DISCRIMINATION PROBABILITY

The theoretical maximum for the probability p in the case of the above states ρ_0 and ρ_1 is obtained as a weighted average of those corresponding to the different eigenspaces of the angular momentum. In fact, for each value of m, the electron states are pure, $|\chi_{0,m}\rangle$ and $|\chi_{1,m}\rangle$, and define a two-level system, within which one can apply the expression of the Helstrom bound. The probabilities that weight the average and normalize the probabilities within each subspace m are the occupation probabilities of each subspace, namely, $p_0q_{0,m} + p_1q_{01,m}$. Therefore,

$$\begin{aligned}p^{\rho}_{\max} &= \sum_m (p_0q_{0,m} + p_1q_{01,m})p^{\psi}_{\max|m} = \frac{1}{2} + \frac{1}{2}\sum_m (p_0q_{0,m} + p_1q_{01,m})\left[1 - \frac{4p_0p_1q_{0,m}q_{1,m}}{(p_0q_{0,m} + p_1q_{1,m})^2}|\langle\chi_{0,m}|\chi_{1,m}\rangle|^2\right]^{\frac{1}{2}} \\ &= \frac{1}{2} + \frac{1}{2}\sum_m \left[(p_0q_{0,m} + p_1q_{1,m})^2 - 4p_0p_1q_{0,m}q_{1,m}|\langle\chi_{0,m}|\chi_{1,m}\rangle|^2\right]^{\frac{1}{2}}.\end{aligned}$$

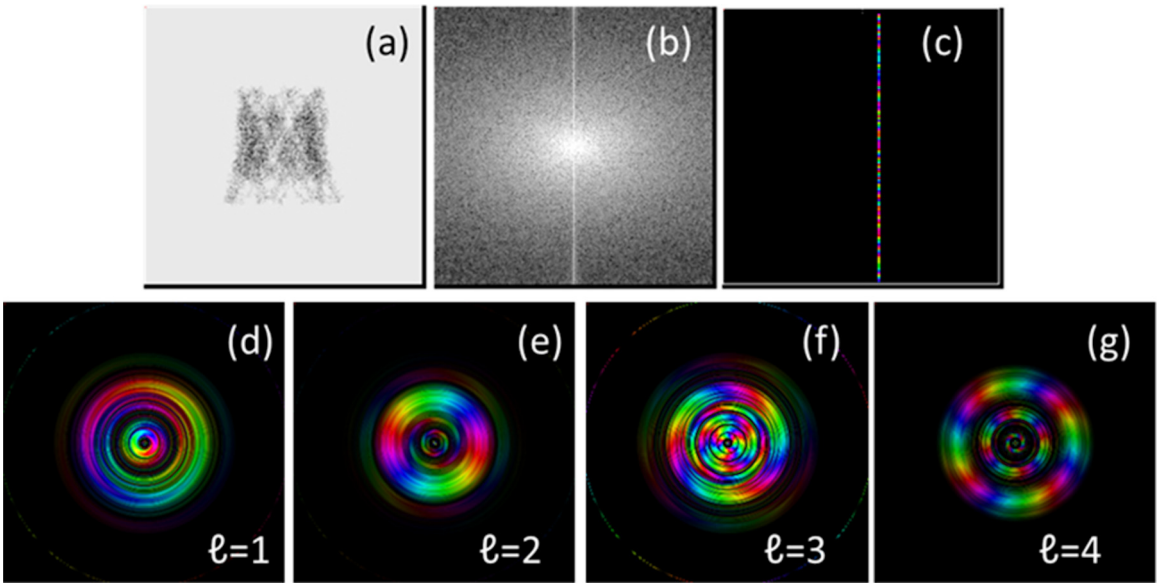

FIG. 3. Example decomposition on special vortex states where the radial part is fitted on the specific protein wave. The initial protein (here we chose the side view as the decomposition does not require the n-fold symmetry) (a) is transformed in log-polar Fourier transform (b) and a single OAM value is selected (c). If the inverse process is done for each OAM we find the single vortex wave (d)–(g).

The probability operators $\pi_{k,m}$ that one can associate with the generalized OAM sorter are diagonal on the basis of the angular momentum eigenstates. Therefore, the probabilities that correspond to each outcome are independent of the phases $\alpha_{k,m}$, and only depend on the amplitudes $q_{k,m}$. From this it follows that, as shown in Eq. (6), also the discrimination probability obtained with the sorter is the same in the pure- and in the mixed electron-state cases.

The optimal observable is obtained by applying the results that are known for the pure-state case to each value of m. In fact, within each subspace, one has to discriminate two pure states, namely, $|\chi_{0,m}\rangle$ and $|\chi_{1,m}\rangle$. The absence of (accessible) coherences between subspaces corresponding to different values of m allows one to treat each subspace independently. The optimal observable is a two-valued observable, whose eigenstates coincide with the eigenstates $|\lambda_{1,m}\rangle$ and $|\lambda_{2,m}\rangle$ of $\sigma_m \equiv \sum_{j=0,1}(-1)^j p_j q_{j,m}|\chi_{j,m}\rangle\langle\chi_{j,m}|$. In practice, the application of phase elements allows one to implement an equivalent measurement for the radial degree of freedom, where one of the eigenstates actually coincides with, e.g., $|\lambda_{1,m}\rangle$, while the complementary subspace is spanned by a finite number of other eigenstates. Hence the presence of a single, dominant peak in the case of one protein, and of a more distributed spectrum in the case of the other (Fig. 2).

APPENDIX C: DECOMPOSITION OF A WAVE IN CORRELATED OAM RADIAL STATES

In this Appendix we report the detail and example of the mathematical decomposition in OAM radial-correlated states. The OAM sorters uses a conformal transformation to lead to the angular basis formed by OAM, indicated by the integer quantum number m, and log-radial momentum here simply indicated as P_ϱ. As a consequence, it transforms a vortex beam into a narrow line that projects to a peak in the OAM subspace. The elongated shape in the orthogonal direction is the effect of the radial distribution for each OAM subspace.

The protein states that we want to decompose must have the form as in Eq. (1). In each OAM subspace the wave is $\psi_m = \chi_m(\rho)\exp(im\varphi)$.

Here, $\chi_m(\rho) = \int \psi_{\rm ew}(\rho,\varphi)\exp(-im\varphi)d\varphi$ and $\psi_{\rm ew}$ is the overall wave function after interacting with the protein. In practice, each $\psi_{\rm ew}$ is a vortex in the azimuthal part but it has a radial function that is fitted to the protein or state to be projected on. We want to show here explicitly the functional shape of the states ψ_m. To do this the target state [Fig. 3(a)] is transformed into log-polar coordinates and then Fourier transposed [Fig. 3(b)]. For this example, we are using a side view of protein P_b. Every vertical stripe corresponds to a single OAM component; it can be isolated [Fig. 3(c)] to produce the special vortex ψ_m and back transformed to Cartesian direct coordinates to show how the single vortex mode looks. Figures 3(d)–3(g) show the ψ_m corresponding to $m = 1, 2, 3, 4$. It should be noted that these vortices are, by construction, orthogonal to each other and to the vacuum.

APPENDIX D: FURTHER EXAMPLES

In this Appendix we report further details on the evolution of the electron wave function after the interaction with the molecule. This induces a phase modulation in the xy plane, which is displayed in Cartesian [Fig. 4(a)] and log-polar coordinates [Fig. 4(b)]. The latter one gives the probability distribution after the interaction with the first element of the OAM sorter. Due to the following propagation, the electron wave function is decomposed into different contributions, corresponding to different values m of L_z [Fig. 4(c)]. Here, additional phase elements, beyond the standard OAM sorter, are introduced in order to perform the *phase flattening*. Finally, a cylindrical lens (produced by the combination of stigmators and round lenses) can be used to obtain a further diffraction

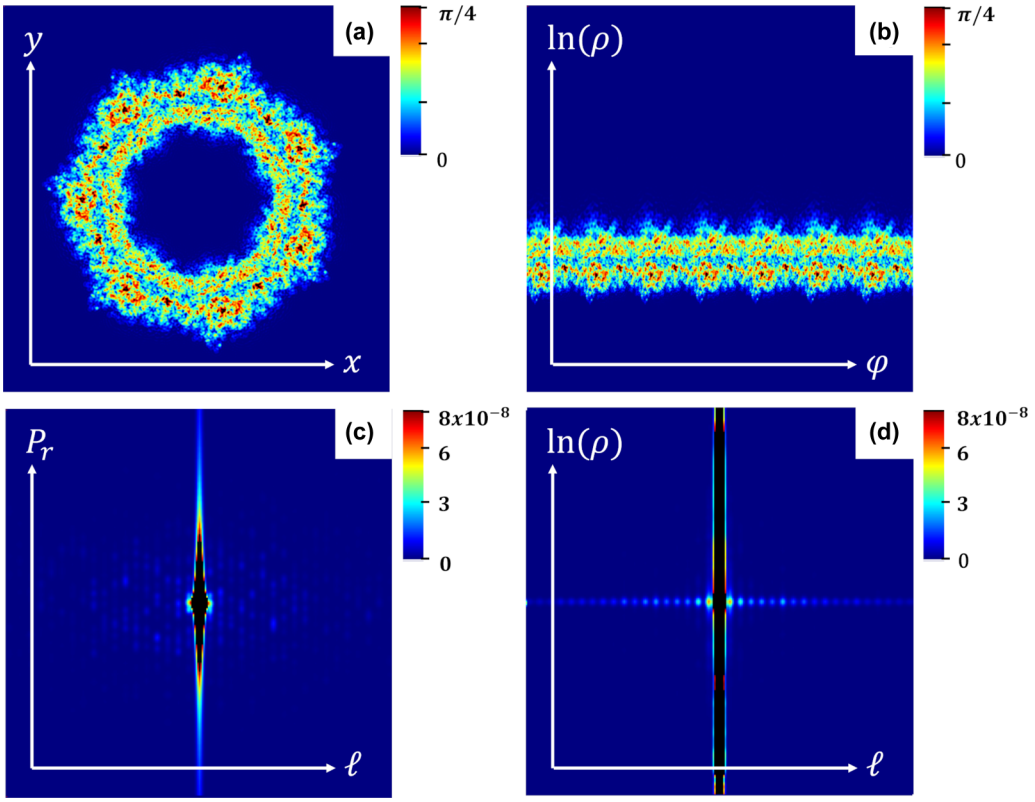

FIG. 4. Series of unitary transformation that the different electrostatic elements apply to the electron wave function in the case of the protein P_a. In particular, we show the phase modulation of the electron wave function in (a) Cartesian and (b) log-polar coordinates. Intensity of the diffraction to the OAM sorter in (c) the radial momentum space and (d) after optimal radial sorting.

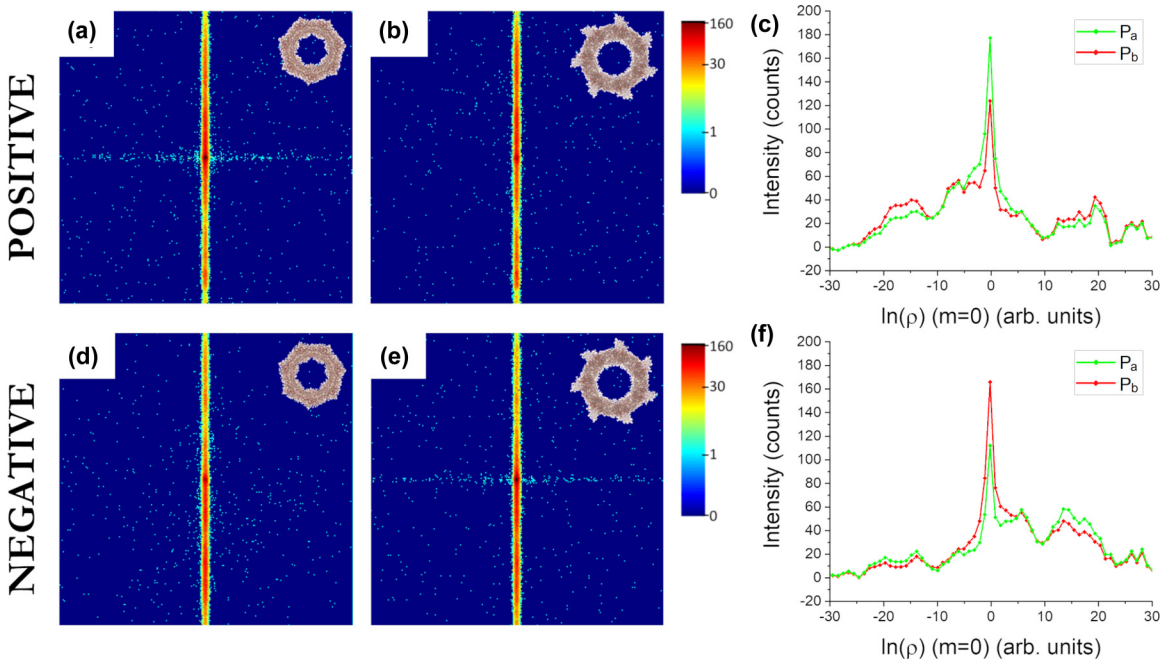

FIG. 5. Discrimination between the proteins P_a and P_b, where the third sorter element implements an optimal measurement. The upper and the lower panels correspond, respectively, to the positive and negative eigenstate. The proteins P_a (a), (d) and P_d (b), (e) give rise to different distributions of the detected electrons in the correlated angular-radial basis. (c), (f) Statistics of the radial observable corresponding to the $m = 0$ subspace, where the electron states are mainly concentrated.

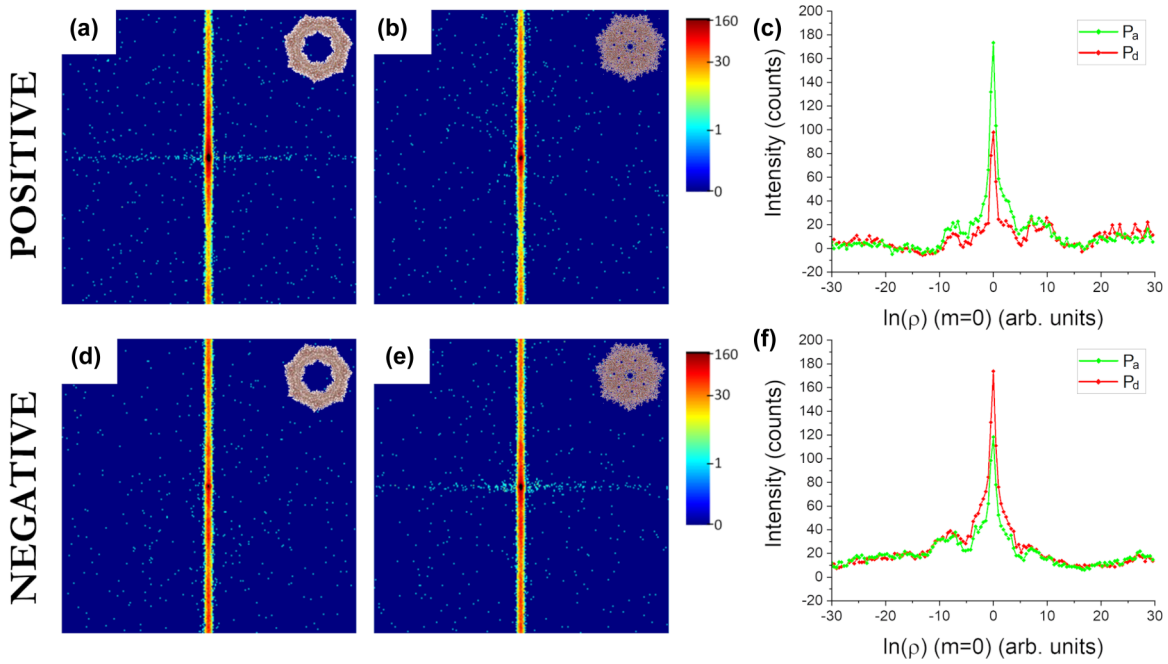

FIG. 6. Discrimination between the proteins P_a and P_d, where the third sorter element implements an optimal measurement. The upper and the lower panels correspond, respectively, to the positive and negative eigenstate. The proteins P_a (a), (d) and P_d (b), (e) give rise to different distributions of the detected electrons in the correlated angular-radial basis. (c), (f) Statistics of the radial observable corresponding to the $m = 0$ subspace, where the electron states are mainly concentrated.

of the radial degree of freedom, while the angular distribution remains unaffected [Fig. 4(d)].

The optimal measurement consists in projecting over the positive or on the negative eigenstate of $\sigma_m \equiv \sum_{j=0,1}(-1)^j p_j q_{j,m}|\chi_{j,m}\rangle\langle\chi_{j,m}|$. It is worth noticing that the discrimination strategy is independent of the choice of the preferred eigenstate as both of them are capable of distinguishing between the two proteins, as demonstrated in Fig. 5.

So far we have tested the optimal discrimination strategy on a precise class of proteins, namely, different configuration of the same molecule. However, the validity of this method is general and can be applied to distinguish between any couple of proteins. As a proof, we reported in Fig. 6 the discrimination between the EspB protein of *Mycobacterium tuberculosis* (labeled as P_a as in the main text) and the Ynal channel of *Escherichia coli* [32] (hereafter labeled as P_d).

[1] C. L. Degen, F. Reinhard, and P. Cappellaro, Rev. Mod. Phys. **89**, 035002 (2017).

[2] M. A. Nielsen and I. L. Chuang, *Quantum Computation and Quantum Information* (Cambridge University Press, Cambridge, 2000).

[3] L. Reimer and H. Kohl, *Transmission Electron Microscopy: Physics of Image Formation and Microanalysis*, (Springer-Verlag, New York, 1993).

[4] R. Henderson, Q. Rev. Biophys. **28**, 171 (1995).

[5] R. Henderson, Proc. Natl. Acad. Sci. USA **110**, 18037 (2013).

[6] M. Radermacher, J. Electron Microsc. Tech. **9**, 359 (1988).

[7] J. Verbeeck, H. Tian, and P. Schattschneider, Nature **467**, 301 (2010).

[8] B. J. McMorran, A. Agrawal, I. M. Anderson, A. A. Herzing, H. J. Lezec, J. J. McClelland, and J. Unguris, Science **331**, 192 (2011).

[9] G. Pozzi, V. Grillo, P. H. Lu, A. H. Tavabi, E. Karimi, and R. E. Dunin-Borkowski, Ultramicroscopy **208**, 112861 (2020).

[10] B. J. McMorran, T. R. Harvey, and M. P. J. Lavery, New J. Phys. **19**, 023053 (2017).

[11] A. H. Tavabi, P. Rosi, G. Pozzi, A. Roncaglia, S. Frabboni, E. Rotunno, P. H. Lu, R. Nijland, P. Tiemeijer, E. Karimi, R. E. Dunin-Borkowski, and V. Grillo, arXiv:1910.03706.

[12] V. Grillo, G. C. Gazzadi, E. Karimi, E. Mafakheri, R. W. Boyd, and S. Frabboni, Appl. Phys. Lett. **104**, 043109 (2014).

[13] V. Grillo, A. H. Tavabi, F. Venturi, H. Larocque, R. Balboni, G. C. Gazzadi, S. Frabboni, P.- H. Lu, E. Mafakheri, F. Bouchard, R. E. Dunin-Borkowski, R. W. Boyd, M. P. J. Lavery, M. J. Padgett, and E. Karimi, Nat. Commun. **8**, 15536 (2017).

[14] G. C. Berkhout, M. P. Lavery, J. Courtial, M. W. Beijersbergen, and M. J. Padgett, Phys. Rev. Lett. **105**, 153601 (2010).

[15] C. W. Helstrom, *Quantum Detection and Estimation Theory* (Academic Press, New York, 1976).

[16] For a recent review, see J. Bae and L.-W. Kweek, J. Phys. A: Math. Theor. **48**, 083001 (2015).

[17] H. Hokamoto, arXiv:2001.05603.

[18] H. Larocque, F. Bouchard, V. Grillo, A. Sit, S. Frabboni, R. E. Dunin-Borkowski, M. J. Padgett, R. W. Boyd, and E. Karimi, Phys. Rev. Lett. **117**, 154801 (2016).

[19] C. W. Helstrom, *Quantum Detection and Estimation Theory* (Academic Press, New York, 1976).

[20] C. L. Schwartz, V. I. Sarbash, F. I. Ataullakhanov, J. R. MacIntosh, and D. Nicastro, J. Micros **227**, 98 (2007).
[21] C. Van Rijnsoever, V. Oorschot, and J. Klumperman, Nat. Methods **5**, 973 (2008).
[22] A. Dudley, T. Mhlanga, M. Lavery, A. McDonald, F. S. Roux, M. Padgett, and A. Forbes, Opt. Express **21**, 165 (2013).
[23] H. Okamoto, T. Latychevskaia, and H.-W. Fink, Appl. Phys. Lett. **88**, 164103 (2006).
[24] L. Reimer, *Transmission Electron Microscopy: Physics of Image Formation and Microanalysis*, 3rd ed. (Springer-Verlag, New York, 1993).
[25] M. Solomonson, Structure **23**, 571 (2015).
[26] An alternative model was developed by A. Gijsbers and R. Ravelli.
[27] F. Zernike, Physica (Amsterdam) **9**, 686 (1942).
[28] R. Danev, B. Buijsse, M. Khoshouei, J. M. Plitzko, and W. Baumeister, Proc. Natl. Acad. Sci. USA **111**, 15635 (2014).
[29] R. Danev and W. Baumeister, Nat. Methods **13**, 395 (2016).
[30] T. Juffmann, S. A. Koppell, B. B. Klopfer, C. Ophus, R. M. Glaeser, and M. A. Kasevich, Sci. Rep. **7**, 1699 (2017).
[31] J. Verbeeck, A. Béché, K. Müller-Caspary, G. Guzzinati, M. A. Luong, and M. Den Hertog, Ultramicroscopy **190**, 58 (2018).
[32] J. Yu, B. Zhang, Y. Zhang, C. Q. Xu, W. Zhuo, J. Ge, J. Li, N. Gao, Y. Li, and M. Yang, Protein Cell **9**, 629 (2018).